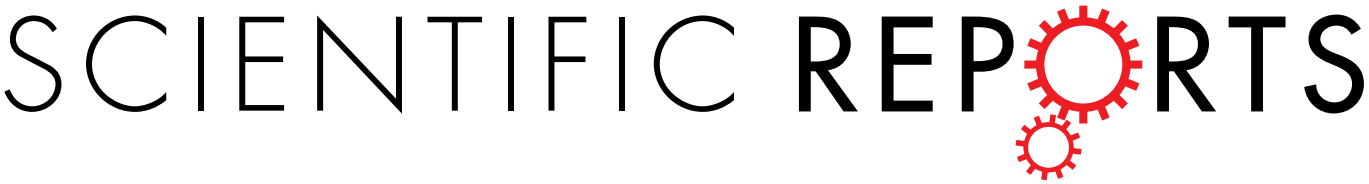

OPEN

Received: 11 July 2016
Accepted: 15 September 2016
Published: 17 October 2016

# Fluorescence-based characterization of non-fluorescent transient states of tryptophan – prospects for protein conformation and interaction studies

Heike Hevekerl*, Johan Tornmalm* & Jerker Widengren

**Tryptophan fluorescence is extensively used for label-free protein characterization. Here, we show that by analyzing how the average tryptophan fluorescence intensity varies with excitation modulation, kinetics of tryptophan dark transient states can be determined in a simple, robust and reliable manner. Thereby, highly environment-, protein conformation- and interaction-sensitive information can be recorded, inaccessible via traditional protein fluorescence readouts. For verification, tryptophan transient state kinetics were determined under different environmental conditions, and compared to literature data. Conformational changes in a spider silk protein were monitored via the triplet state kinetics of its tryptophan residues, reflecting their exposure to an air-saturated aqueous solution. Moreover, tryptophan fluorescence anti-bunching was discovered, reflecting local pH and buffer conditions, previously observed only by ultrasensitive measurements in highly fluorescent photo-acids. Taken together, the presented approach, broadly applicable under biologically relevant conditions, has the potential to become a standard biophysical approach for protein conformation, interaction and microenvironment studies.**

Tryptophan (Trp) auto-fluorescence is widely used for label-free structural and dynamic studies of proteins[1], and Room Temperature Phosphorescence (RTP) from the Trp triplet state can provide valuable complementary information[2–7]. In contrast to Trp fluorescence, which decays within nanoseconds after excitation, RTP lifetimes of Trp can vary from microseconds to seconds. This gives an extended time window for protein dynamics studies, and makes RTP a sensitive readout of local rigidity, environment and of exposure to intrinsic or extrinsic quenchers. However, compared to fluorescence, the phosphorescence signal is much weaker, and for useful RTP measurements all triplet state deactivation processes other than phosphorescence typically have to be suppressed. This requires careful sample deoxygenation and understanding of the mechanisms governing the Trp triplet state lifetime. The triplet state of Trp and other indole compounds have been extensively characterized by RTP[8–13] and Flash Photolysis (FP)[14–17], where the triplet state lifetime is determined by time-resolved triplet-triplet absorption measurements following light excitation. Depending on methodology, and most likely on differences in sample preparation, reported intersystem crossing rates of Trp, Trp triplet state lifetimes and quenching rates of different compounds have been found to differ by more than an order of magnitude[8–17].

As an alternative to RTP and FP, Fluorescence Correlation Spectroscopy (FCS) can be used to determine population kinetics of triplet[18] and other long-lived, non-fluorescent states of fluorescent molecules[19–21], via changes in the detected fluorescence intensity from a limited number of fluorescent molecules at a time. For such studies, FCS combines the high environmental sensitivity and long observation time-window of the long-lived non-fluorescent states, with the high detection sensitivity following from the use of fluorescence as the readout signal. However, FCS measurements require the studied molecules to display high fluorescence brightness. Trp

Royal Institute of Technology (KTH), Dept Applied Physics, Experimental Biomolecular Physics, Albanova Univ Center, 106 91 Stockholm, Sweden. *These authors contributed equally to this work. Correspondence and requests for materials should be addressed to J.W. (email: jwideng@kth.se)

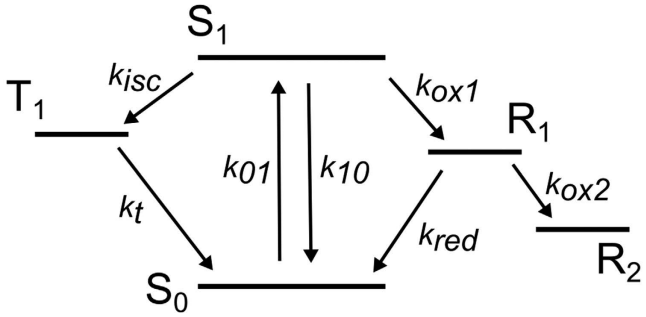


**Figure 1. Basic electronic state model of Trp used in this study.** $S_0$ and $S_1$ denote the ground and first excited singlet state, with the excitation and deactivation rates denoted by $k_{01}$ and $k_{10}$. From $S_1$ intersystem occurs with a rate $k_{isc}$ to the lowest triplet state, $T_1$, which in turn decays with a rate $k_t$ back to $S_0$. Photo-ionization of Trp is assumed to take place from $S_1$ with a rate $k_{ox1}$. The formed radical, $R_1$, can then either return to $S_0$ via reduction (with rate $k_{red}$), or go into a more long-lived non-fluorescent state $R_2$. For Trp[14–17], as well as for organic fluorophores in the visible range[21,36,38], photoionization has been reported to be both mono- and bi-photonic in nature. In this study however, the applied laser excitation intensities were relatively low, and excitation to higher excited states, and subsequent bi-photonic ionization, can therefore be neglected. For fluorophores in general, subsequent photo-ionization to $R_1$ may in principle also occur from $T_1$, as reported e.g. for rhodamine dyes in polyvinlyalcohol[60]. In our experiments on Trp, this alternative photo-oxidation pathway is kinetically indistinguishable from $S_1$ photo-oxidation (see Results). However, since previous studies of Trp photophysics have concluded that photo-oxidation takes place from $S_1$ only[14,15,17,29,32,39], we use this pathway of photo-oxidation in our model.

fluorescence is thus typically too weak for FCS studies, and has only been possible to use for crude diffusion studies of large proteins or aggregates, containing hundreds of Trps[22,23].

In this study, we introduce transient state monitoring (TRAST) as a means to characterize non-fluorescent photo-induced states of Trp. In TRAST, the time-averaged fluorescence intensity from a sample subject to time-modulated excitation is recorded[24]. By analyzing how the recorded average fluorescence intensity varies with the excitation modulation characteristics, in particular the pulse duration, kinetic information of photo-induced, non-fluorescent transient states can be obtained. Like FCS, TRAST combines the detection sensitivity of fluorescence with the environmental sensitivity of long-lived non-fluorescent states. However, TRAST is not dependent on the detection of fluorescence fluctuations from individual molecules, and is therefore not restricted to studies of molecular species with high fluorescence brightness. In contrast to RTP, the fluorescence signal is relatively insensitive to impurities, and TRAST measurements do not require deoxygenation or careful control of quenchers. With relaxed requirements on sample preparation, detection quantum yield and time-resolution of the instrument, as well as on fluorescence brightness of the molecules studied, TRAST is broadly applicable, and has been demonstrated both for solution measurements[25,26] and live cell studies[27,28]. This far, the studies have been based on fluorescence from added fluorophores. In this work, we introduce label-free TRAST spectroscopy in the ultra-violet wavelength range, applied to Trp transient state and protein conformation studies. By TRAST, we revisit the transient state kinetics of Trp in aqueous solutions, establish an electronic state model, investigate the influence of pH, oxygen, ascorbic acid, potassium iodide and various buffers, and compare the determined rates for triplet state formation/decay and photo-oxidation with those reported from RTP and FP measurements. Under acidic conditions, we identify a negative relaxation term in the detected fluorescence at onset of excitation, which we attribute to a delayed fluorescence anti-bunching, caused by excitation-induced proton transfer (EPT). Upon variation of pH and buffer concentration, the amplitude and relaxation time of this negative term was found to reflect the protonation state of Trp and the buffer-mediated recovery rates of Trp following EPT. Finally, TRAST was also demonstrated for protein studies. Conformational changes in a spider silk protein could be monitored via the triplet state kinetics of its Trp residue, reflecting its accessibility to molecular oxygen in a surrounding air-saturated aqueous solution. Taken together, our studies show that TRAST can record a whole set of transient state parameters, yielding environment-, protein conformation- and interaction-sensitive information, not retrievable via traditional protein fluorescence readouts. The presented approach offers a robust alternative to RTP, FP and traditional protein auto-fluorescence readouts for label-free micro-environmental monitoring, as well as for structural and dynamic studies of proteins, and is applicable under a broad range of biologically relevant conditions.

## Results

**Validation of Trp electronic state model –excitation irradiance and oxygen concentration dependence.** Figure 1 shows the basic electronic state model used in this work. It is based on major features of Trp transient state transitions, as reported in literature[5,6,9,10,13–17,29], and agrees with basic models used to analyse TRAST data of xanthene dyes in the visible wavelength range[25,26]. To validate the model, and to investigate how TRAST spectroscopy compares to RTP and FP for determining dark state transitions in Trp, TRAST curves of Trp in buffer solution were recorded under different excitation irradiances, under air-saturated and deoxygenated conditions (Fig. 2). In the TRAST curves (normalized time-averaged fluorescence intensity detected within

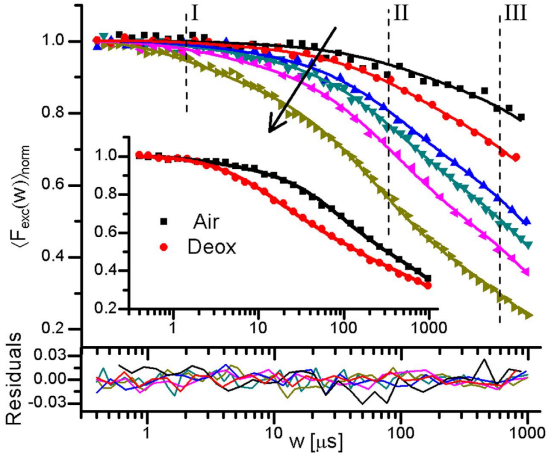


**Figure 2. Normalized TRAST curves (dotted) recorded from a buffered 5 μM Trp solution (pH 7.4, 40 mM TRIS) using average $I_{exc}$ of 4.8, 9.2, 14, 17, 28, and 65 kW/cm² (black arrow indicate increasing $I_{exc}$).** Fitted curves (lines) generated as described in the main text, with residuals (bottom). Inset: TRAST curves recorded in air-saturated (black) and de-oxygenated (red) solutions, $I_{exc} = 28\,kW/cm^2$. Fitted curves (lines) generated as described in the main text.

an excitation pulse, $\langle F_{exc}(w)\rangle_{norm}$, plotted versus pulse duration, $w$, see Methods), three relaxation processes could be distinguished, within $w = 2$–$3\,\mu s$ (I), 60–100 μs (II), and in the sub-ms time range (III). These relaxation processes agree well with the three excitation-induced dark states in the electronic state model of Fig. 1, specifically since their amplitudes tend to increase and their relaxation times decrease with higher excitation intensities. Upon oxygen removal, a prominent increase of both the amplitude and the relaxation time of process (I) can be noticed in the TRAST curves (Fig. 2, inset), consistent with oxygen as an efficient quencher of the Trp triplet state[14,15]. Based on the rate equations and initial condition of Eq. 2, and using Eq. 9, rate parameters were numerically fitted to the TRAST curves (procedure described in the Methods section). The two curves (Fig. 2, inset) were fitted simultaneously, with the parameters $k_{isc}$, $k_{ox1}$, $k_{red}$ and $k_{ox2}$ set global for the curves, and only $k_t$ allowed to be different between the curves. The fitted curves could well reproduce the experimental TRAST curves (inset Fig. 2, fitted parameter values in Supplementary Table 1). From this fitting procedure, $k_{isc}$ was determined to $28\,\mu s^{-1}$. A fluorescence lifetime of Trp, $\tau_f = 3$ ns[30,31], yields a triplet quantum yield of $q_T = 0.084$, which is in the middle of the relatively broad range of $q_T$ values reported from RTP or FP studies: 0.0065[10], 0.065[15], 0.09[32], 0.14[33], 0.24[17]. $k_t$ was determined to $k_t(deoxy) = 0.094\,\mu s^{-1}$ in the deoxygenated solution, corresponding to a triplet decay time of $\tau_T(deoxy) = 11\,\mu s$, and to $k_t(air) = 0.74\,\mu s^{-1}$ in the air-saturated sample. Our value of $\tau_T(deoxy)$, is in line with values obtained by FP (10 μs[15], 14 μs[14] and 43 μs[34]), while RTP lifetimes of Trp under similar conditions have been reported to be as long as 1.2 ms[8]. From the difference $k_t(air) - k_t(deoxy) = 0.65\,\mu s^{-1}$, and with approximately 0.24 mM of dissolved molecular oxygen in the air-saturated aqueous solution, we get a $T_1$ quenching rate by oxygen of $2.7 \cdot 10^9\,M^{-1}s^{-1}$. This is somewhat lower than previously reported for Trp ($\sim 5 \cdot 10^9\,M^{-1}s^{-1}$ [14,15]), but higher than for organic fluorophores ($\sim 2 \cdot 10^9\,M^{-1}s^{-1}$ [18]). Given that the quenching rate for both the organic fluorophores and for Trp can be expected to be mainly determined by oxygen diffusion ($D \sim 2 \cdot 10^{-5}\,cm^2/s$ [35]), our determined $k_t$ values seem reasonable. Oxygen, as an electron acceptor, can likely also promote the $k_{ox1}$ rate, and a difference between the $k_{ox1}$ rates in air-saturated and in deoxygenated aqueous solutions would then be expected. However, given a determined $k_{ox1}$ rate in the range of $10^7\,s^{-1}$ (see below), the relative contribution to $k_{ox1}$ from diffusion-controlled photo-oxidation of $S_1$ by molecular oxygen is limited to a few percent and is within the experimental uncertainty of our measurements.

The TRAST curves of Fig. 2 were analyzed similarly to those in the inset, with all six curves fitted simultaneously. Given the generally low amplitudes of the relaxation process attributed to $T_1$ relaxation (I), $k_{isc}$ was fixed to $28\,\mu s^{-1}$, as determined from the curves in the inset. $k_t$, $k_{red}$ and $k_{ox2}$ were set global, and $k_{ox1}$ was allowed to vary between the curves. The fitted curves could then well reproduce all the experimental TRAST curves, further confirming that the model in Fig. 1 adequately describes the observed dark state transitions of Trp. From the fitting, $k_t = 0.71\,\mu s^{-1}$, well in agreement with the value determined for the inset curves. $k_{ox1}$ was determined within a relatively confined range for the different curves, from 5.7 to $9.4\,\mu s^{-1}$, corresponding to a photo-ionization quantum yield of $q_{ox} = 0.017$–$0.028$. $k_{red} = 0.011\,\mu s^{-1}$ and $k_{ox2} = 0.002\,\mu s^{-1}$. Our determined $q_{ox}$ values for Trp are considerably higher than for organic fluorophores in aqueous solution under comparable excitation conditions[36]. This may be a consequence of the higher excitation energies involved in the photo-induced electron transfer[37]. On the other hand, the determined $q_{ox}$ range is lower than previously determined $q_{ox}$ values of Trp by FP under comparable conditions (0.04[15], 0.075[17], 0.08[14], 0.14[32], 0.16[16], 0.25[29]). This can partly be attributed to diffusion effects, with Trp in long-lived transient states in the detection volume being replaced by fresh Trp outside of the volume. Previous simulations of TRAST experiments[38] have shown that state transitions slower than the probe molecule diffusion through the detection volume can lead to a two-fold under-estimation of the transition rates to a dark state ($k_{ox1}$), and over-estimations of up to a factor of five of dark-state recovery rates ($k_{red}$). Taking diffusion into account, we can thus estimate $q_{ox} = 0.03$–$0.06$, i.e. at the lower end among the previously reported values,

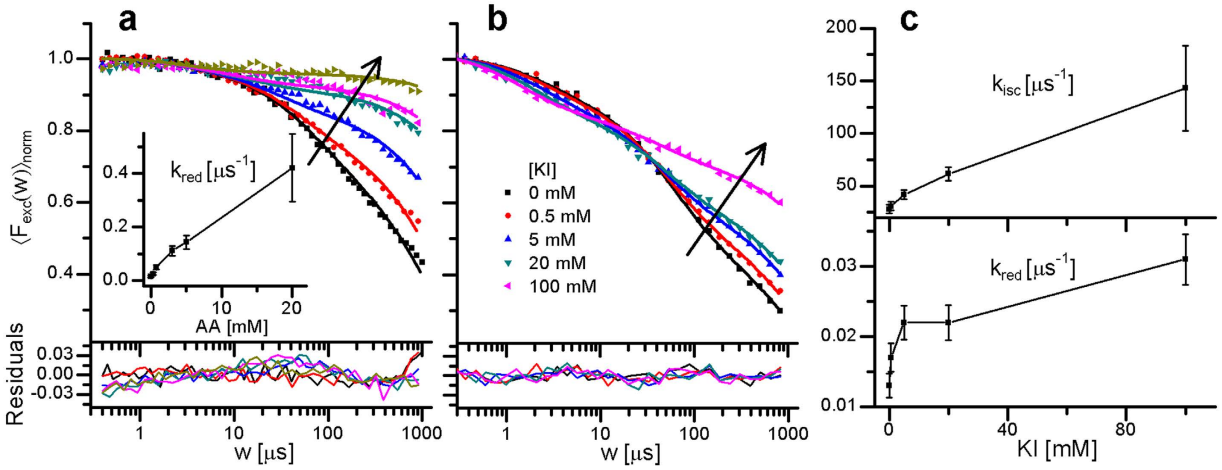


**Figure 3. Normalized TRAST curves recorded from Trp in 40 mM Tris buffer, pH 7.4 (dotted).** Fitted curves (lines) with residuals (bottom) generated as described in the main text. **(a)** Ascorbic acid (AA) titration, with [AA] from 0 to 20 mM. Black arrow indicates increasing [AA]. $I_{exc} = 17\,kW/cm^2$. Inset: Fitted $k_{red}$ values vs [AA]. Error bars denote 95% confidence intervals. **(b)** Potassium iodide (KI) titration, with [KI] from 0 to 100 mM ($I_{exc} = 65\,kW/cm^2$). **(c)** Top: Fitted $k_{isc}$ values vs [KI], Bottom: Fitted $k_{red}$ values vs [KI], with error bars denoting 95% confidence intervals.

and $k_{red}$ to be as low as $2\,ms^{-1}$ in the absence of Trp reductants in the solution. For comparison, we also fitted the TRAST curves in Fig. 2 and in the inset of Fig. 2 to a model, assuming photo-oxidation to occur also from $T_1$, with the same rate as from $S_1$. The quality of fit was as good as when assuming photo-oxidation from $S_1$ only. This alternative model is kinetically indistinguishable from the model of Fig. 1, and results in considerably lower $k_{ox1}$ rates ($0.18\,\mu s^{-1}$ and $0.025\,\mu s^{-1}$, in the air-saturated and in the deoxygenated samples, respectively). However, since many studies of Trp photophysics favor photo-oxidation from $S_1$ only[14,15,17,29,32,39], we hereinafter used the model of Fig. 1 to analyse our data.

**Effects of reductants and quenchers.** *Ascorbic acid.* To verify that relaxation process (II) in the TRAST curves is mainly a consequence of Trp photo-oxidation, and to investigate how the photodynamics of Trp are affected by the presence of reducing agents, we added ascorbic acid (AA) in different concentrations ([AA] = 0–20 mM) and performed TRAST measurements at low excitation irradiances ($I_{exc} = 17\,kW/cm^2$) to suppress triplet state build-up. With higher [AA], a prominent reduction of the dark state build-up was evident from the recorded TRAST curves (Fig. 3a). Simultaneous fitting, with $k_{isc}$ and $k_t$ fixed to values determined above (28 and $0.74\,\mu s^{-1}$, respectively), $k_{ox1}$ and $k_{ox2}$ set global for all curves, and with $k_{red}$ allowed to take individual values for each curve, resulted in fitted curves well reproducing the experimental curves (fitted parameter values given in Supplementary Table 1). The globally fitted $k_{ox1}$ and $k_{ox2}$ values (10 and $0.0039\,\mu s^{-1}$) agree well with the values determined for the curves in Fig. 2. The $k_{red}$ parameter values, individually fitted to each TRAST curve, showed a close to linear dependence on [AA] (inset, Fig. 3a), with a quenching constant of $k_{Qred}(AA) = 2.5 \cdot 10^7\,M^{-1}s^{-1}$. This confirms that photo-oxidation strongly contributes to the dark state build-up of Trp in our measurements, that the photo-oxidized state $R_1$ is sensitive to reducing agents, and indicates that relative changes of $k_{ox1}$ and $k_{red}$ can be accurately monitored. It can be noted that the $k_{Qred}(AA)$ determined for Trp is about two orders of magnitude lower than that determined for the organic dye Rhodamine 6G (Rh6G)[36], and also that there is no obvious enhancement of photo-induced reduction upon addition of reductants in mM concentrations, as found for e.g. Rh6G[36,40].

*Potassium iodide (KI).* For organic fluorophores in the visible wavelength range, KI can influence both the triplet state and act as a fluorophore reducing agent, contributing to the recovery of photo-oxidized dyes back into viable fluorophores[40]. By the heavy atom effect, KI enhances $k_{isc}$ for almost all dyes with excitation in the visible wavelength range, but can also enhance $k_t$ by means of electron transfer for dyes with excitation maximum in the blue-green range[40]. To investigate how the transient states of Trp are affected, TRAST curves were recorded from Trp in buffer solution, with different KI concentrations added ([KI] = 0–100 mM) (Fig. 3b). KI was found to influence both the $T_1$ and $R_1$ kinetics of Trp. Simultaneous fitting, with $k_{isc}$ and $k_{red}$ allowed to take individual values for each curve, $k_{ox1}$ and $k_{ox2}$ set global for all curves, and with $k_t$ fixed to the determined value ($0.74\,\mu s^{-1}$) for 0 mM KI and then assumed to increase linearly with [KI] with a quenching constant $k_{Qt}$, resulted in fitted curves well reproducing the experimental curves (fitted parameter values given in Supplementary Table 1). In the fitting, a total quenching rate of $S_1$ ($k_{isc}$ included) by KI of $3.9 \cdot 10^9\,M^{-1}s^{-1}$, as reported from steady-state and time-resolved fluorescence measurements of Trp[10], was included in the $k_{10}$ rate. The individually fitted $k_{isc}$ values show a close to linear dependence on [KI] (Fig. 3c), and linear regression yields $k_{isc} + k_{Qisc}\cdot[KI] = 34\,\mu s^{-1} + 1.1 \cdot 10^9\,M^{-1}s^{-1}\cdot[KI]$. For $k_{red}$ a less pronounced linearity was found. $k_{Qt}$ was determined to $2.9 \cdot 10^6\,M^{-1}s^{-1}$. In comparison to bimolecular quenching constants determined for organic dyes in the visible range, the determined $k_{Qisc}$ is similar as for Rhodamine Green (RhGr)[40], but one order of magnitude lower than for Rh6G[18]. Similar to AA, $k_{Qred}$ for KI is

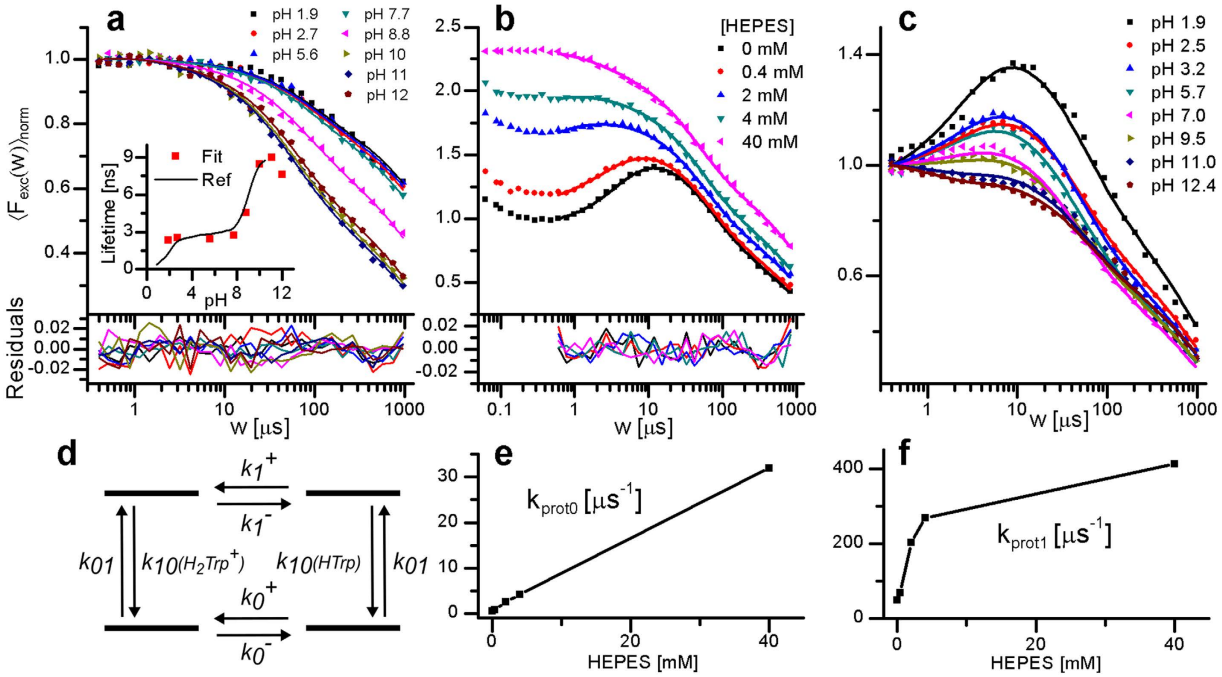


**Figure 4.** (**a**) TRAST curves recorded from Trp in a 40 mM TRIS buffer at different pH (dotted). $I_{exc} = 14\,kW/cm^2$. Fitted curves (lines) with residuals (bottom) generated as described in the main text. Fitted parameter values: $k_{isc} = 15\,\mu s^{-1}$, $k_{ox1} = 8.6\,\mu s^{-1}$, $k_{red} = 13\,ms^{-1}$ and $k_{ox2} = 2.1\,ms^{-1}$ (see text for details). Inset: The individually fitted values for $1/k_{10}$ (red circles), plotted vs pH together with the fluorescence lifetimes determined in refs 30 and 31 (black line). (**b**) Normalized average fluorescence intensity $\langle F_{exc}(w)\rangle_{norm}$ of Trp in $H_2O$ with different concentrations of HEPES (relative amplitudes between the curves preserved), pH 1.9, $I_{exc} = 89\,kW/cm^2$. Fitted curves (lines) with residuals (bottom) generated as described in the main text. (**c**) $\langle F_{exc}(w)\rangle_{norm}$ of Trp in $H_2O$ at different pH (1.9–12.4) in the absence of buffer, $I_{exc} = 43\,kW/cm^2$. (**d**) Protonation model for $S_0$ and $S_1$, added to the model of Fig. 1 in the analysis of the TRAST curves in Fig. 4b. (**e**) Protonation relaxation rate in $S_0$, $k_{prot0}$, determined from the TRAST curves in Fig. 4b, plotted versus the HEPES buffer concentration. Error bars denote 95% confidence intervals. (**f**) Corresponding protonation relaxation rate in $S_1$, $k_{prot1}$, plotted versus [HEPES]. Error bars denote 95% confidence intervals.

about two orders of magnitude lower than the corresponding quenching constant for a Rhodamine fluorophore (RhGr)[40], and there are no indications of a photo-induced reduction of Trp upon addition of mM concentrations of KI, as observed for organic dyes in the visible range[40]. This observation, and the different $k_{Qisc}$ and $k_{Qt}$ between visible-range fluorophores themselves, and between these fluorophores and Trp, reflect differences in redox potentials and in $S_1$ and $T_1$ energy levels. Given the reported total quenching rate of $S_1$[10], our value of $k_{Qisc}$ indicates that only a minor part of the KI-mediated quenching of $S_1$ takes place via intersystem crossing to $T_1$.

**Effects of pH and buffer concentration.** *pH effects in buffer solution.* The influence of pH on the transient state population dynamics of Trp was investigated by recording TRAST curves from Trp in a 40 mM TRIS buffer over a wide pH range (1.9–12.1). The excitation irradiance was kept low ($I_{exc} = 14\,kW/cm^2$) to minimize triplet state build-up. In the recorded TRAST curves (Fig. 4a), the amplitude of the relaxation process II was found to be almost constant for pH 1.9–7.7, increase for pH 7.7–11.1 and then decrease slightly for pH 12.1. Rate parameters were fitted to the curves as above, based on the model of Fig. 1. The eight curves were fitted globally, but given the strong pH dependence of the $k_{10}$ rate reported[30–32], also the $k_{10}$ rate was fitted, and was allowed to take individual values for each curve. The $k_{isc}$, $k_{ox1}$, $k_{ox2}$ and $k_{red}$ rates were globally fitted for all curves, and the $k_t$ rate was fixed to $0.74\,\mu s^{-1}$, as determined above. The fitted curves could well reproduce the experimental data (Fig. 4a), with the globally fitted rates (given in the figure caption) in reasonable agreement with those determined above, and with the individually fitted $k_{10}$ rates found to comply very well with previously reported fluorescence lifetimes[30–32] (inset, Fig. 4a). The variation of radical state formation with different pH can thus be explained by the strong pH dependence of the Trp fluorescence lifetime, $\tau_F = 1/k_{10}$, where higher $k_{10}$ rates result in lower $q_T$ and $q_{ox}$ values.

*pH- and buffer-dependent initial decay and fluorescence anti-bunching.* For Trp in low pH (1.9) solutions, with no or sub-mM buffer concentrations present, an initial (<200–300 ns) decay in the TRAST curves is followed by a distinct negative relaxation term for $w = 0.5$–$10\,\mu s$. Both the initial decay and the negative term were found to decrease in amplitude with increasing buffer concentrations (Fig. 4b) and pH (Fig. 4c). The pH dependence and time range of the initial decay suggest that it reflects formation of a previously reported, short-lived (~26 ns)

triplet state of Trp[14,15], protonated at its excited indole ring. The fast relaxation of this state was partly beyond the time resolution of our TRAST measurements, and we did not investigate the kinetics of this state further. Instead, we focused on the negative relaxation term, and analyzed the TRAST curves for pulse durations beyond this initial decay. Negative relaxation terms attributed to anti-bunching[41] have previously been observed in single molecule fluorescence and FCS measurements[42–45], with relaxation rates given by the sum of $k_{01}$ and $k_{10}$ (Methods, Eq. 4). For Trp, this would correspond to relaxation times in the ns time range, three orders of magnitude faster than what we observe. Given the clear dependence on both buffer concentration (Fig. 4b) and pH (Fig. 4c), the slow anti-bunching is likely due to excitation-induced proton transfer (EPT). EPT for Trp[39,46–48] can take place due to different $pK_a$ values of ground state Trp ($S_0$), with $pK_a$ values of 2.4–2.6[14,47] and 9.4[14,49], and excited state Trp ($S_1$), with $pK_a^*$ values not so precisely determined, but possibly shifted from the ground-state $pK_a$ values by several pH units[1,49,50]. The slow anti-bunching was modelled by including reversible proton exchange for both $S_0$ and $S_1$, as depicted in Fig. 4d, into the model of Fig. 1. The $k_{10}$ rates for $H_2Trp^+$ and HTrp were fixed to 1/(1 ns) and 1/(3 ns), respectively[30,31]. In the overall model, all other rates to and from $S_0$ and $S_1$ are assumed to be the same, irrespective of the state of protonation, in agreement with previous data for intersystem crossing[32] and photo-oxidation[14]. The slow anti-bunching relaxation time at low pH and low buffer concentrations reflects the time it takes to reach a new equilibrium after onset of excitation, between the weakly fluorescent, double-protonated form $H_2Trp^+$ and the more fluorescent single-protonated form HTrp (Fig. 4b). The negative relaxation amplitude in the TRAST curves indicates that $pK_a > pK_a^*$, which at onset of excitation shifts the balance between HTrp and $H_2Trp^+$ in favor of HTrp, resulting in an increase in fluorescence intensity. The observed behavior of Trp, with a photon antibunching relaxation time far longer than seen in single-molecule experiments on fluorophores[41–45] (Eq. 4), is similar to that recently observed in single-molecule experiments on highly fluorescent photo-acids[51,52]. Rate parameters were fitted to the curves in Fig. 4b, based on the model of Fig. 1, adding the possibility of proton exchange in $S_0$ and $S_1$ (Fig. 4d), with $k_t$ and $k_{isc}$ fixed to the values determined above ($0.74\,\mu s^{-1}$ and $28\,\mu s^{-1}$), $k_{ox1}$ and $k_{ox2}$ fitted as global parameters, and $k_{red}$ allowed to take individual values for each curve. Since the curves were recorded at the same pH (1.9) with different buffer concentrations, we assumed the ratios of the protonation on- and off- rates in $S_0$ and $S_1$, $k_0^+/k_0^-$ and $k_1^+/k_1^-$, to have common values. These ratios were thus fitted as global parameters for all curves. In contrast, the protonation relaxation rates for $S_0$ and $S_1$, $k_{prot0} = k_0^+ + k_0^-$ and $k_{prot1} = k_1^+ + k_1^-$, can be expected to vary with the buffer concentration and were fitted individually to each of the curves. The fitted $k_{prot0}$ values show a linear dependence with $k_{prot0} = 0.8{\cdot}10^6\,s^{-1} + 0.8{\cdot}10^9\,M^{-1}s^{-1}{\cdot}$[HEPES] (Fig. 4e). This indicates a diffusion-controlled proton exchange in $S_0$ with a similar bimolecular rate constant as for e.g. fluorescein in buffer solutions[53]. In contrast, the buffer concentration dependence of $k_{prot1}$ shows a more complex behavior. The fitted values for $k_{prot1}$ are generally an order of magnitude higher than for $k_{prot0}$ and tend to increase with higher buffer concentrations. The far higher, apparently not diffusion-limited, proton exchange rates within $S_1$ may be explained by excitation-induced intramolecular proton transfer (EIPT), reported to take place from the protonated amino group of Trp to the excited indole ring[1,32,39,46,48,50]. However, transitions between rotamer states of Trp, having different potential surfaces in $S_0$ and $S_1$[54] can also contribute to the observed behavior. The ratios $k_0^+/k_0^-$ and $k_1^+/k_1^-$ were globally fitted to 8.7 and 0.15, which with a pH of 1.9 yields an estimated $pK_a$ of 2.8 and a $pK_a^*$ of 1.1. The $pK_a$ value is a bit higher than previously reported (2.6[47], 2.4[14]), but the difference $pK_a$-$pK_a^* = 1.7$ is in line with suggested differences between the $S_0$ and $S_1$ states of Trp[1,49,50]. The other rate parameters fitted for the curves in Fig. 4b were found to be well in agreement with the previously determined parameter values (Supplementary Table 1). For the highest buffer concentration studied (40 mM), the influence of the proton exchange in $S_0$ and $S_1$ on the TRAST curves is negligible, which supports that it can be neglected in the analysis of the TRAST curves in Fig. 4a (recorded at 40 mM TRIS buffer).

*pH-dependence in absence of buffer.* In the set of TRAST curves in Fig. 4c, measured at different pH with no buffer added, the negative anti-bunching relaxation observed in the TRAST curves at lower pH gradually disappears with higher pH, and for TRAST curves recorded at high pH a small positive relaxation process is instead observed in the μs time range. The observed general trend cannot be fit into our simple model, and quantitative curve fitting of the TRAST curves based on a more advanced model goes beyond the scope of this work. However, the observed trend can likely be understood as a combination of different $pK_a$ values of $S_0$ and $S_1$, presence of EIPT and possible transitions between different Trp rotamer states. The molecular brightness, or $q_f$, of Trp is pH-dependent and closely follows the variation of $\tau_f$, as depicted in Fig. 4a[30,31,47], with distinct increases in $q_f$ at pH ~ 2.5 ($pK_a$ of the COOH group of Trp) and at pH ~ 9.4 ($pK_a$ of the $NH_3^+$ group of Trp). For the low pH transitions ($H_2Trp^+$ - HTrp), we concluded that $pK_a > pK_a^*$. Onset of excitation then favors HTrp over $H_2Trp^+$, and with $q_f(\text{HTrp}) > q_f(H_2Trp^+)$ a relaxation term with negative amplitude in the TRAST curves can be generated. In the mid-pH range ($2.5 \ll \text{pH} \ll 9.4$), a negative relaxation term in the μs time-range is still observed in the TRAST curves (Fig. 4c). This cannot be attributed to differences in $pK_a$ and $pK_a^*$, which are both far outside this pH-range. However, also in this pH-range, there is clear evidence for several Trp excited state reactions, including proton transfer, electron transfer and rotamer interconversions[55]. EIPT (from the $NH_3^+$ group to the excited indole ring of Trp) have been reported[32,46,47] and may arise as a consequence of an increase of the $pK_a$ of the indole nitrogen upon excitation. The efficiency of EIPT can depend on the rotamer state of Trp. Equilibria between different Trp rotamer states have been found to be different in $S_0$ and in $S_1$[54,56], and if excitation favors rotamers with higher fluorescence quantum yields, this can result in the pH-dependent negative relaxation terms observed in our measurements. However, it should be noted that despite extensive studies, the transitions between different Trp rotamers and how they influence the fluorescence properties of Trp are still not fully understood[55]. A more precise explanation of our observations in the mid-pH range based on these transitions is thus difficult to give and is also beyond the scope of this study. For pH > 9.4, above the $pK_a$ of the $NH_3^+$ group, EIPT from $NH_2$ does not occur, and as a consequence no negative relaxation term is observed in this pH range (Fig. 4c). At this pH range however, transitions between HTrp and $Trp^-$ can occur, and $q_f(Trp^-) > q_f(\text{HTrp})$. The decreased fluorescence at

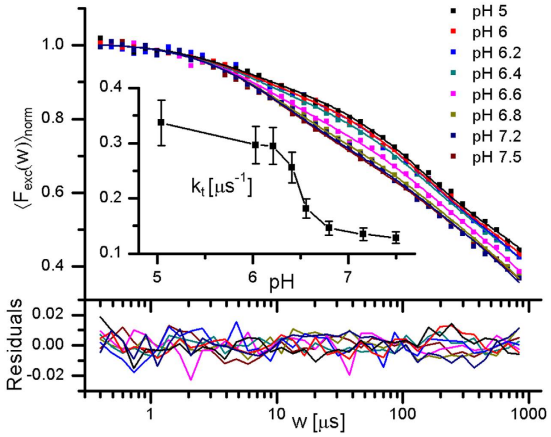


**Figure 5. TRAST curves recorded at moderate excitation irradiance ($I_{exc}$ = 9.2 kW/cm²) from a sample of 4 μM NT dissolved in 20 mM TRIS, with pH varied from 5 to 7.5.** Fitted curves (lines) with residuals (bottom) generated as described in the main text. Inset: Fitted $k_t$ rates, plotted versus pH. Error bars denote 95% confidence intervals.

onset of excitation, with a positive relaxation term in the μs time-range in the TRAST curves (Fig. 4c), may suggest that $pK_a < pK_a^*$ for this transition. This agrees with a previously estimated $pK_a^*$ of 12–13[1], and that the less fluorescent HTrp is then favored over $Trp^-$ at onset of excitation. However, triplet state build-up can also not be fully excluded as a reason for this positive relaxation term.

**Protein measurements.** Given the sensitivity of the Trp transient states to the immediate environment, as displayed from the TRAST experiments, we investigated to what extent this could be exploited to monitor protein conformational changes.

TRAST experiments were performed on the N-terminal (NT) domain of the Major ampulate spidroin (MaSp), an extensively characterized spider silk protein[57]. NT contains ~130 residues and a single Trp residue buried in its core. MaSp can transform into insoluble fibres, induced by a pH change (pH 7 → 6) in a well defined region of the silk glands[56]. In this process, NT is proposed to act as a pH-regulated relay, conferring solubility at high pH and facilitating fibre formation at low pH. NT is mainly monomeric at pH 7 and dimeric at pH 6, and upon monomer to dimer interconversion the single Trp residue relocates from the inner core to a more solvent-exposed environment[57].

We monitored this interconversion of NT by TRAST experiments, performed over a pH range of 5–7.5 (Fig. 5). For pH 7.5–7.2, the recorded TRAST curves were close to identical, displaying two major decay processes: a first process with a lifetime of 5–10 μs and a second, slower process present for $w > 100$ μs. With further reduced pH, from 7.1 to 6.1, lower amplitudes and faster decays for the first decay process were observed. For pH 6 and lower, again close to identical curves were recorded. The observed differences were found to be reversible, as the TRAST curve at pH 7.2 (black curve in Fig. 5), recorded after the low pH measurements, fully resembled the initial TRAST curves recorded in the upper pH range. All TRAST curves were subject to global analysis, based on the model of Fig. 1, with $k_{isc}$, $k_{ox1}$ and $k_{red}$ fitted as global parameters for all curves, and $k_t$ and $k_{ox2}$ allowed to take individual values for the different curves. The fitted curves were found to well reproduce the experimental curves (Fig. 5). While the determined values of $k_{ox1}$ (16 $\mu s^{-1}$) and $k_{red}$ (7.3 $ms^{-1}$) were relatively similar to those for free Trp in aqueous solution (Fig. 2a), $k_{isc}$ was found to be about a factor of four higher (99 $\mu s^{-1}$). In proteins, local rigidity and quenching moieties close to the site of the indole ring have been found to strongly affect Trp phosphorescence lifetimes[5,11,58]. The influence of these factors on $k_{isc}$ is difficult to investigate by RTP measurements, and also with FP, where the small changes in the transmitted optical radiation make it difficult to resolve different contributions and their kinetics[11]. However, these factors are believed to also influence the phosphorescence quantum yield, including $k_{isc}$[6]. Together with the increased rigidity experienced by Trp when confined with peptide bonds in the protein, this can explain the higher $k_{isc}$ observed for NT, compared to that found for free Trp in aqueous solution. The $k_t$ rates, individually fitted to each of the TRAST curves, are plotted versus pH in the inset of Fig. 5. For low pH, with NT in a dimeric form and with Trp at the solvent-exposed surface, $k_t \sim 0.4\ \mu s^{-1}$. In the higher pH range on the other hand, with NT in a monomeric form and with Trp buried in the interior of the protein, $k_t$ is significantly lower (0.15 $\mu s^{-1}$). In the mid-pH range, $k_t$ smoothly decreases with higher pH, with a half-range transition between the states at pH ~ 6.4. This is perfectly in agreement with a transition between the monomeric and dimeric form of NT at a pH of 6.1–6.5 (depending on the salt concentration), as determined by a combination of CD, NMR, Fluorescence cross-correlation spectroscopy and steady-state fluorescence measurements[57]. The found pH dependence of $k_t$ is also well in agreement with the structural changes predicted for NT[57], where the changes in $k_t$ most likely can be attributed to changes in oxygen accessibility upon protein conformational changes. At the higher pH, the low $k_t$ values indicate that oxygen quenching of the buried Trp is limited. At lower pH, $k_t$ approaches 0.4 $\mu s^{-1}$, in agreement with an expected higher oxygen quenching of the Trp triplet state at the protein surface. This $k_t$ rate is approximately half of that for free Trp in air-saturated aqueous solution (Fig. 2a). This complies with an expected $2\pi$ solid angle of exposure of Trp to the solution, when at the

protein surface, compared to a $4\pi$ solid angle when free in solution. Also for the values of $k_{ox2}$, individually fitted to each curve, a transition in the rate values was found, with a mid-transition pH coinciding with that for $k_t$. This likely also reflects the monomer to dimer transition of NT. However, a similar transition can also be seen for $k_{red}$ and $k_{ox1}$, if fitted individually instead of $k_{ox2}$. One can therefore not directly assign this transition to a specific physical change in any of the $k_{ox1}$, $k_{ox2}$ or $k_{red}$ rates. As a verification that the observed changes were caused by a protein conformation change of NT, and not by any pH influence on the Trp residue itself, only a minor increase in $\langle F_{exc}(w)\rangle_{norm}$ was found for free Trp in 40 mM TRIS buffer over the same pH range (Fig. 4a), and mainly at $w > 1$ ms, i.e. not in the time range of the triplet state relaxation.

## Discussion

In this study, transient state transitions of Trp in aqueous solution were determined by TRAST measurements. Starting from a simplified electronic state model, sets of TRAST curves were globally analyzed, with most of the rate parameter values either fixed or set global, and allowing model flexibility and parameter inter-relationships to be included. With a robust experimental approach, and analyses of the recorded curves with a limited number of free variables, transition rates of triplet and photo-oxidized states were identified and determined under different environmental conditions. Taking analyte diffusion into account for the slower transitions, all determined rates were found to be within the range of parameter values reported from FP and RTP measurements. For slower transitions already known, the influence of diffusion on the related relaxations in the TRAST curves can also provide a measure of the mobility of the analyzed molecules[59]. TRAST measurements can thus retrieve similar, and in some aspects extended, transient state information compared to RTP and FP, and can be performed under a broad range of conditions. The instrumentation is relatively simple, and can be further simplified, e.g. by replacing the frequency-tripled UV laser used for excitation in this work with a turn-key CW laser. Apart from the kinetics of triplet and photo-oxidized states, our TRAST measurements also revealed a pH- and buffer-dependent anti-bunching in the Trp fluorescence, previously only observed in specific, highly fluorescent photo-acids, requiring single-molecule or FCS measurements[51,52]. With its relatively much weaker fluorescence, anti-bunching in Trp fluorescence, or any transient state kinetics of Trp, is practically impossible to observe by FCS and single-molecule measurements. By TRAST, the observed anti-bunching can likely also be found in weakly fluorescent compounds other than Trp, having different $pK_a$ and $pK_a^*$ values, providing information about local pH and buffer conditions.

In the NT protein measurements, the triplet state kinetics of its Trp residue was found to reflect the conformational state of the protein in a sensitive and accurate manner. Apart from offering a substitute to FP and RTP, this shows that Trp TRAST measurements can provide additional, highly environment sensitive parameters, extending the information available from traditional protein auto-fluorescence studies. Taken together, based on a robust and simple approach, applicable under a broad range of biologically relevant conditions, Trp TRAST measurements have the potential to become a standard biophysical approach for protein conformation, interaction and microenvironment studies.

## Methods

**Population dynamics in the electronic state model of Trp at onset of excitation.** In the electronic state model of Fig. 1, only $S_1$ generates fluorescence, upon decay to $S_0$, and the emitted fluorescence intensity, $F(t)$ is thus proportional to the $S_1$ population, $S_1(t)$:

$$F(t) = k_{10} q_f S_1(t) \tag{1}$$

with $q_f$ denoting the fluorescence quantum yield. For a Trp molecule subject to constant excitation starting at $t = 0$, and with the electronic state model in Fig. 1, the population probabilities of the electronic states can be described by:

$$\frac{d}{dt}\begin{pmatrix} S_0(t) \\ S_1(t) \\ T_1(t) \\ R_1(t) \\ R_2(t) \end{pmatrix} = \begin{pmatrix} -\sigma\cdot\Phi_{exc} & k_{10} & k_t & k_{red} & - \\ \sigma\cdot\Phi_{exc} & -(k_{10}+k_{isc}+k_{ox1}) & - & - & - \\ - & k_{isc} & -k_t & - & - \\ - & k_{ox1} & - & -(k_{red}+k_{ox2}) & - \\ - & - & - & k_{ox2} & - \end{pmatrix} \cdot \begin{pmatrix} S_0(t) \\ S_1(t) \\ T_1(t) \\ R_1(t) \\ R_2(t) \end{pmatrix},$$

$$\text{with the initial condition: } \begin{pmatrix} S_0(t) \\ S_1(t) \\ T_1(t) \\ R_1(t) \\ R_2(t) \end{pmatrix} = \begin{pmatrix} 1 \\ 0 \\ 0 \\ 0 \\ 0 \end{pmatrix} \tag{2}$$

Here, $\sigma$ denotes the excitation cross section, and $\Phi_{exc}$ the excitation photon flux, with $\Phi_{exc} = \frac{I_{exc}}{h\nu}$, where $I_{exc}$ is the excitation intensity and $h\nu$ the excitation photon energy, so that $k_{01} = \sigma\cdot\Phi_{exc}$. $S_1(t)$ can then in a general form be described by:

$$S_1(t) = \frac{\sigma\cdot\Phi_{exc}}{\sigma\cdot\Phi_{exc}+k_{10}}\left[1 - e^{-\lambda_{ab}t} - \sum_{i=1}^{p}[A_i - A_i e^{-\lambda_i t}]\right], \tag{3}$$

where $p$ denotes the number of different photo-induced non-fluorescent states involved (states other than $S_0$ and $S_1$). $\lambda_{ab}$ and $\lambda_i$ are the eigenvalues, i.e. the rates of the relaxation modes of $S_1(t)$ upon onset of constant excitation, and $A_i$ the related amplitudes, reflecting the population build-up of the different photo-induced non-fluorescent states. For most fluorescent molecules, equilibration between $S_0$ and $S_1$ after onset of excitation takes place within the time range of the fluorescence lifetime (ns), while the dark state relaxations ($1/\lambda_i$) typically occur on a μs-ms time scale. The $S_0$-$S_1$ equilibration time, referred to as the anti-bunching time[41–44] $\tau_{ab} = 1/\lambda_{ab}$, is typically given by[45]:

$$\tau_{ab} = \frac{1}{\sigma \cdot \Phi_{exc} + k_{10}} \tag{4}$$

Based on Eq. 3, $\lambda_i$ and $A_i$ can be described analytically, as functions of the rate parameters of the model in Fig. 1 [20,27,28,40].

**Transient State (TRAST) spectroscopy.** In TRAST spectroscopy, the population dynamics of non-fluorescent, long-lived transient states of fluorescent molecules in a sample is determined from the average fluorescence intensity from the sample, when subject to different excitation pulse trains. We applied square-wave excitation pulse trains in a confocal setup, as described below. For a sample of fluorescent molecules, subject to an excitation pulse train with $n$ pulses of duration $w$ and period $T$, the detected time-averaged fluorescence, $\langle F(w)\rangle$, can then be expressed as[24–28]:

$$\langle F(w)\rangle = \frac{1}{n \cdot T} \iiint c q_D q_f CEF(\bar{r}) k_{10} \sum_{i=1}^{n} \left( \int_0^w S_{1,i}(\bar{r}, t)\, dt \right) dV \tag{5}$$

Here $n{\cdot}T$ is the total duration of the excitation pulse train, $c$ the concentration of the fluorescent species, $q_D$ the overall detection quantum yield of the instrument, and $CEF$ the collection efficiency function of the confocal setup. The term $S_{1,i}(\bar{r}, t)$ denotes the probability that a fluorescent molecule, located at $\bar{r}$ in the confocal detection volume, is in its excited singlet state at time $t$ after on-set of the $i$:th excitation pulse. Dividing $\langle F(w)\rangle$ with the pulse train duty cycle ($\eta = w/T$) yields the average fluorescence intensity within an excitation pulse:

$$\langle F_{exc}(w)\rangle = \langle F(w)\rangle/\eta \tag{6}$$

$\langle F_{exc}(w)\rangle$ normalized to 1 for pulse durations $|\lambda_{ab}| \ll w \ll |\lambda_i|$, denoted $\langle F_{exc}(w)\rangle_{norm}$, represents the averaged population of $S_0$ and $S_1$, within the pulse duration, and over the detection volume:

$$\langle F_{exc}(w)\rangle_{norm} = \langle S_0(w) + S_1(w)\rangle = \frac{\iiint CEF(\bar{r}) \frac{\sigma \cdot \Phi_{exc}(\bar{r}) + k_{01}}{\sigma \cdot \Phi_{exc}(\bar{r})} \left( \frac{1}{w} \int_0^w S_{1,i}(\bar{r}, t)\, dt \right) dV}{\iiint CEF(\bar{r})\, dV} \tag{7}$$

With knowledge of $I_{exc}(\bar{r}) = h\upsilon\Phi_{exc}$, $CEF(\bar{r})$, and the electronic state model (Eq. 2), and by use of Eq. 7, the pulse duration dependence of $\langle F_{exc}(w)\rangle$, making up a so-called TRAST-curve, can be used to extract the transient state rate parameters, as previously shown for organic fluorophores[24–28]. Approximating the average excitation rate in the detection volume by:

$$\bar{k}_{01} = \frac{\int \sigma \cdot \Phi_{exc}(\bar{r}) \bar{S}_1(\bar{r}) CEF(\bar{r})\, dV}{\int \bar{S}_1(\bar{r}) CEF(\bar{r})\, dV}, \tag{8}$$

where $\bar{S}_1(\bar{r}) = \sigma \cdot \Phi_{exc}(\bar{r})/(k_{10} + \sigma \cdot \Phi_{exc}(\bar{r}))$, i.e. the $S_1$ population at onset of excitation, after equilibration between the singlet states, but before dark state build-up. A simplified expression for $\langle F_{exc}(w)\rangle$ can then be obtained, given by

$$\langle F_{exc}(w)\rangle_{norm} = \frac{1}{w} \int_0^w \frac{k_{10} + \bar{k}_{01}}{\bar{k}_{01}} S_1(t)\, dt, \tag{9}$$

with $S_1(t)$ given by Eqs 2 and 3, or modified according to any other electronic state model than in Fig. 1.

**Instrumentation and measurement procedure.** TRAST measurements were performed on a home-built, epi-illuminated, confocal microscope setup, with excitation from a mode-locked Ti:Sapphire laser (Mira 900, Coherent, Inc., pumped by a Nd:Vanadate laser (Verdi$^{TM}$ V-10, Coherent, Inc.), operating at 870 nm, pulse width ~120 fs FWHM, 76 MHz repetition rate), frequency-tripled with a third harmonic generator (INRAD M/N 5-050, Inrad Inc.) to 290 nm. The mirrors (BHR-2506U-280, Lambda Research Optics Inc.) between the third harmonic generation system and the microscope also served as an excitation filter (reflection at 245–330 nm). The frequency-tripled laser beam was adjusted with a continuously-variable neutral density filter (Thorlabs), intensity-modulated by an acousto-optic modulator (AOM; MQ200-B80A1-266, AA Opto-Electronics, Orsay, Cedex), and was then focused into the sample by a microscope objective (Ultrafluar 100/1.25 glyc, Zeiss). From FCS measurements of 2-aminopurine in aqueous solution, the $1/e^2$ radius of the laser beam in the focal plane was determined to 445 nm. Fluorescence from the sample was collected through the same objective, separated from excitation light by a dichroic beamsplitter (FF310-Di01, Semrock, Inc.), focused onto a 75 μm diameter pinhole in the image plane and was then spectrally filtered (357/44 nm bandpass filter, Semrock). The fluorescence was then split by a polka dot beamsplitter (50:50, Thorlabs), focused and then detected by two

single photon counting photomultiplier tubes (H7360-02, Hamamatsu), the signals of which were recorded with a PCI-6602 counter/timer card (National Instruments Corp.) for subsequent TRAST analysis (see below).

Square-wave excitation pulse trains were applied in the setup described above. TRAST curves were generated by recording $\langle F_{exc}(w)\rangle$ for up to 30 different excitation pulse trains, with the pulse width $w$ varied between 60 ns and 10 ms. The height of the pulses, that is the excitation irradiance, was kept at a constant level, as indicated below. The duty cycle $\eta$ was kept at 1% to ensure a complete relaxation of tryptophan to the ground singlet state and/or renewal of tryptophan by diffusion at the onset of the next excitation pulse. The total duration of each excitation pulse train $n \cdot T$ was between 1 and 10 s.

**Data analysis.** Data analysis was performed using software implemented in Matlab. The experimental data was pre-processed by subtracting detector dark counts and adjusting for detector dead time. Drifts in sample concentration, arising from a combination of bleaching and evaporation were corrected for by repetitive reference measurements throughout each experiment, using the shortest available pulse width to avoid buildup of any dark states. For the experiments with tryptophan in solution, the effect of bleaching was negligible and the evaporation in most cases small, about 0.5%. For certain longer measurements however, the total evaporation was as large as 5%.

In order to fit the data to a chosen photophysical model, simulated TRAST curves were generated by calculating $\langle F_{exc}(w)\rangle$ from Eq. 5 for each pulse width, $w$, then normalized to $\langle F_{exc}(w)\rangle_{norm}$ (Eqs 6 and 7), if not stated otherwise. The excitation rate, $k_{01}(\bar{r}) = \sigma \cdot \Phi_{exc}(\bar{r})$, using an excitation cross section of $\sigma = 1.26 \cdot 10^{-17}\,\mathrm{cm}^2$, can be estimated assuming a three-dimensional Gaussian distribution of $\Phi_{exc}(\bar{r})$, with a beam radius ($1/e^2$) of 454 nm and an axial extension of 3 μm. However, the benefits of including a full 3D Gaussian excitation beam, with $k_{01}(\bar{r})$ varying throughout the confocal volume, together with the microscope collection efficiency function $CEF(\bar{r})$ were found to be small. Great improvement in computational speed, without sacrificing much accuracy, could be achieved by instead approximating an average excitation rate in the detection volume, $\overline{k}_{01}$, given by Eq. 8.

The remaining model parameters were then optimized using Eq. 9, and an iterative non-linear least square approach to match the calculated curves to the experimental data. Multiple TRAST curves could also be fitted simultaneously, with each rate being specified as global or independent between curves.

The simulations also used an adjusted value for the pulse widths, $w$. A small but constant shift in pulse duration, $\Delta w$, caused by non-zero rise- and fall-times of the AOM, lead to a relative error in illumination time given by $\Delta w/w$. With $\Delta w$ in the order of 10 ns, and constant for all pulse widths, this effect is only relevant for the shortest pulses.

**Sample preparation.** A new stock solution of 1 mM L-tryptophan was freshly prepared for each day of measurements and was further diluted to 2–10 μM in double distilled water (Barnstead EASYpure UV/UF, reagent grade water system), TRIS (Trizma base), HEPES, phosphate buffer ($NaH_2PO_4$, $Na_2HPO_4$) or NaCl solution. The pH was set to pH 7.4 with NaOH and HCl, if not stated otherwise. Ascorbic acid and potassium iodide were added in the concentrations stated in the text. Spider silk protein (kind gift from Dr. N. Kronqvist and Prof. J. Johansson, Karolinska Institute, Stockholm, Sweden) was dissolved in 20 mM TRIS buffer to 4 μM concentration and the pH was varied from pH 7.5–5.0 with NaOH and HCl. All chemicals were purchased from Sigma Aldrich. Deoxygenation experiments were performed in a sealed container, where the solution was bubbled with nitrogen gas for twenty minutes before measurements. During the experiment, a low flow of nitrogen was applied over the sample to avoid re-oxygenation.

## References


1. Engelborghs, Y. The analysis of time resolved protein fluorescence in multi-tryptophan proteins. *Spectrochim Acta Part A* **57,** 2255–2270 (2001).
2. Saviotti, M. L. & Galley, W. G. Room temperature Phosphorescence and the Dynamic Aspects of Protein Structure. *Proc. Natl. Acad. Sci. USA* **71(10),** 4154–4158 (1974).
3. Vanderkooi, J. M., Calhoun, D. B. & Englander, S. W. On the prevalence of room-temperature protein phosphorescence. *Science* **236,** 568–569 (1987).
4. Buscaglia, M., Kubelka, J., Eaton, W. A. & Hofrichter, J. Determination of ultrafast protein folding rates from loop formation dynamics. *J. Mol. Biol.* **347,** 657–664 (2005).
5. Subramaniam, V., Gafni, A. & Steel, D. G. Time-resolved tryptophan phosphorescence spectroscopy: a sensitive probe of protein folding and structure. *IEEE J. Selected Topics in Quant. Electron*. **2,** 1107–1114 (1996).
6. Vanderkooi, J. M. & Berger, J. W. Excited triplet states used to study biological macromolecules at room temperature. *BBA-Bioenergetics* **976,** 1–27 (1989).
7. Gonnelli, M. & Strambini, G. B. Phosporescence lifetime of tryptophan in proteins. *Biochemistry* **34,** 13847–13857 (1995).
8. Strambini, G. B. & Gonnelli, M. Tryptophan Phosphorescence in Fluid Solution. *J. Am. Chem. Soc.* **117,** 7646–7651 (1995).
9. Kowalska-Baron, A., Galecki, K. & Wysocki, S. Temperature study of indole, tryptophan and N-acetyl-L-tryptophanamide (NATA) triplet-state quanchng by iodide in aqueous solution. *Spectrochim Acta Part A* **111,** 42–48 (2013).
10. Kowalska-Baron, A., Chan, M., Galecki, K. & Wysocki, S. Photophysics of indole, tryptophan and N-acetyl-L-tryptophanamide (NATA): Heavy atom effect. *Spectrochim Acta Part A* **98,** 282–289 (2012).
11. Gershenson, A., Gafni, A. & Steel, D. Comparison of the time-resolved absorption and phosphorescence from the tryptophan triplet state in proteins in solution. *Photochem. Photobiol.* **67,** 391–398 (1998).
12. Strambini, G. B., Kerwin, B. A., Mason, B. D. & Gonnelli, M. The triplet lifetime of indole derivatives in aqueous solution. *Photochem. Photobiol.* **80,** 462–470 (2004).
13. Fischer, C. J., Gafni, A., Steel, D. G. & Schauerte, J. A. The triplet lifetime of indole in aqueous and viscous environments: significance to the interpretation of room temperature phosphorescence in proteins. *J. Am. Chem. Soc.* **124,** 10359–10366 (2002).
14. Bent, D. V. & Hayon, E. Excited state chemistry of aromatic amino acids and related peptides. III. Tryptophan. *J. Am. Chem. Soc.* **97,** 2612–2619 (1975).
15. Tsentalovich, Y. P., Snytnikova, O. A. & Sagdeev, R. Z. Properties of excited states of aqueous tryptophan. *J. Photochem. Photobiol. A* **162,** 371–379 (2004).
16. Klein, R., Tatischef, I., Bazin, M. & Santus, R. Photophysics of indole. Comparative study of quenching, solvent, and temperature effects by laser flash photolysis and fluorescence. *J. Phys. Chem.* **85,** 670–677 (1981).

17. Bazin, M., Patterson, L. K. & Santus, R. Direct observation of monophotonic photoionization in tryptophan excited by 300-nm radiation. A laser photolysis study. *J. Phys. Chem.* **87,** 189–191 (1983).
18. Widengren, J., Mets, Ü. & Rigler, R. Fluorescence correlation spectroscopy of triplet states in solution: A theoretical and experimental study. *J. Phys. Chem.* **99,** 13368–13379 (1995).
19. Widengren, J. & Schwille, P. Characterization of photoinduced isomerization and back-isomerization of the cyanine dye Cy5 by fluorescence correlation spectroscopy. *J. Phys. Chem. A*. **104(27),** 6416–6428 (2000).
20. Widengren, J., Dapprich, J. & Rigler, R. Fast interactions between Rh6G and dGTP in water - a fluorescence correlation spectroscopy study. *Chem. Phys.* **216,** 417–426 (1997).
21. Eggeling, C., Widengren, J., Rigler, R. & Seidel, C. Photobleaching of Fluorescent Dyes under Conditions used for Single-Molecule-Detection: Evidence of Two-Step Photolysis. *Anal. Chem.* **70,** 2651–2659 (1998).
22. Lippitz, M., Erker, W., Decker, H., van Holde, K. E. & Basché, T. Two-photon excitation microscopy of tryptophan-containing proteins. *Proc. Natl. Acad. Sci. USA* **99,** 2772–2777 (2002).
23. Sahoo, B., Balaji, J., Nag, S., Kumar Kaushalya, S. & Maiti, S. Protein aggregation probed by two-photon fluorescence correlation spectroscopy of native tryptophan. *J. Chem. Phys.* **129,** 075103-1-5 (2008).
24. Widengren, J. Fluorescence-based transient state monitoring for biomolecular spectroscopy and imaging. *J Royal Soc Interface*, **7(49),** 1135–1144 (2010).
25. Sandén, T., Persson, G., Thyberg, P., Blom, H. & Widengren, J. Monitoring kinetics of highly environment-sensitive states of fluorescent molecules by modulated excitation and time-averaged fluorescence intensity recording *Anal. Chem.* **79(9),** 3330–3341 (2007).
26. Sandén, T., Persson, G. & Widengren, J. Transient state imaging for microenvironmental monitoring by laser scanning microscopy. *Anal. Chem.* **80,** 9589–9596 (2008).
27. Chmyrov, V., Spielmann, T., Hevekerl, H. & Widengren, J. Trans–Cis Isomerization of Lipophilic Dyes Probing Membrane Microviscosity in Biological Membranes and in Live Cells. *Anal. Chem.* **87**, 5690–5697 (2015)
28. Spielmann, T., Xu, L., Gad, A. K. B., Johansson, S. & Widengren, J. Transient State Microscopy Probes Patterns of Altered Oxygen Consumption in Cancer Cells. *FEBS J*. **281,** 1317–1332 (2014).
29. Dudley Bryant, F., Santus, R. & Grossweiner, L. I. Laser flash photolysis of aqueous tryptophan. *J. Phys. Chem.* **79,** 2711–2716 (1975).
30. Jameson, D. M. & Weber, G. Resolution of the pH-dependent heterogeneous fluorescence decay of tryptophan by phase and modulation measurements. *J. Phys. Chem.* **85,** 953–958 (1981).
31. Gudgin, E., Lopez-Delgado, R. & Ware, W. R. The tryptophan fluorescence lifetime puzzle. A study of decay times in aqueous solution as a function of pH and buffer conditions. *Can. J. Chem.* **59,** 1037–1044 (1981).
32. Robbins, R. J. *et al.* Photophysics of aqueous tryptophan: pH and temperature effects. *J. Am. Chem. Soc.* **102,** 6271–6279 (1980).
33. Chen, Y., Liu, B., Yu, H. T. & Barkley, M. D. The peptide bond quenches indole fluorescence. *J. Am. Chem. Soc.* **118,** 9271–9278 (1996).
34. Lapidus, L. J., Eaton, W. E. & Hofrichter, J. Measuring the rate of intramolecular contact formation in polypeptides. *Proc. Natl. Acad. Sci. USA* **97,** 7220–7225 (2000).
35. Han, P. & Bartels, D. M. Temperature dependence of oxygen diffusion in $H_2O$ and $D_2O$. *J. Phys. Chem.* **100,** 5597–5602 (1996).
36. Widengren, J., Chmyrov, A., Eggeling, C., Löfdahl, P. Å. & Seidel, C. A. M. Strategies to improve photostability in ultrasensitive fluorescence spectroscopy. *J. Phys. Chem. A* **111(3),** 429–440 (2007).
37. Rehm, D. & Weller, A. Kinetics of fluorescence quenching by electron and H-atom transfer. *Isr. J. Chem.* **8,** 259–271 (1970).
38. Spielmann, T., Blom, H., Geissbuehler, M., Lasser, T. & Widengren, J. Transient state monitoring by total internal reflection fluorescence microscopy. *J. Phys. Chem. B*, **114,** 4035–4046 (2010).
39. Sherin, P. S., Snytnikova, O. A. & Tsentalovich, Y. P. Tryptophan photoionization from prefluorescent and fluorescent states. *Chem. Phys. Lett.* **391,** 44–49 (2004).
40. Chmyrov, A., Sandén, T. & Widengren, J. Iodide as a fluorescence quencher and promoter – mechanisms and possible implications. *J. Phys. Chem. B*, **114(34),** 11282–11291 (2010).
41. Kimble, H. J., Dagenais, M. & Mandel, L. Photon antibunching in resonance fluorescence. *Phys. Rev. Lett.* **39,** 691–695 (1977).
42. Ehrenberg, M. & Rigler, R. Rotational Brownian diffusion and fluorescence intensity fluctuations. *Chem. Phys.* **4,** 390–401 (1974).
43. Kask, P., Piksarv, P. & Mets, Ü. Fluorescence correlation spectroscopy in the nanosecond time range – photon antibunching in dye fluorescence. *Eur. Biophys. J.* **12,** 163–166 (1985).
44. Basché, T., Moerner, W. E., Orrit, M. & Talon, H. Photon antibunching in the fluorescence of a single dye molecule trapped in a solid. *Phys. Chem. Lett.* **69,** 1516–1519 (1992).
45. Mets, Ü., Widengren, J. & Rigler, R. Application of the antibunching in dye fluorescence: measuring the excitation rates. *Chem. Phys.* **218,** 191–198 (1997).
46. Yu, H. T., Colucci, W. J., Mclaughlin, M. L. & Barkley, M. D. Fluorescence quenching in indoles by excited-state proton transfer. *J. Am. Chem. Soc.* **114,** 8449–8454 (1992).
47. Lehrer, S. S. Deuterium isotope effect on the fluorescence of tryptophan in peptides and in lysozyme. *J. Am. Chem. Soc.* **92,** 3459–3462 (1970).
48. Shizuka, H., Serizawa, M., Shimo, T., Saito, I. & Matsuura, T. Fluorescence-quenching mechanism of tryptophan. Remarkable efficient internal proton-induced quenching and charge transfer quenching. *J. Am. Chem. Soc.* **110,** 1930–1934 (1988).
49. Chang, M. C., Petrich, J. W., McDonald, D. B. & Fleming, G. R. Nonexponential fluorescence decay of tryptophan, tryptophylglycine, and glycyltryptophan. *J. Am. Chem. Soc.* **105,** 3819–3824 (1983).
50. Chen, Y. & Barkley, M. D. Toward understanding tryptophan fluorescence in proteins. *Biochem.* **37,** 9976–9982 (1998).
51. Vester, M., Staut, T., Enderlein, J. & Jung, G. Photon antibunching in a cyclic chemical reaction scheme. *J. Phys. Chem. Lett.* **6,** 1149–1154 (2015).
52. Vester, M., Grueter, A., Finkler, B., Becker, R. & Jung, G. Biexponential photon antibunching: recombination kinetics within the Förster-cycle in DMSO. *Phys. Chem. Chem. Phys.* **18,** 10281–10288 (2016).
53. Widengren, J., Terry, B. & Rigler, R. Protonation kinetics of GFP and FITC investigated by FCS - aspects of the use of fluorescent indicators for measuring pH. *Chem. Phys.* **249,** 259–271 (1999).
54. Szabo, A. G. & Rayner, D. M. Fluorescence decay of tryptophan conformers in aqueous solution. *J. Am. Chem. Soc.* **102,** 554–563 (1980).
55. Liu, B. *et al. cis*-1-amino-2-(3-indoyl)cyclohexane-1-carboxylic acid: A single tryptophan Chi1 rotamer model. *J. Am. Chem. Soc.* **124,** 13329–13338 (2002).
56. Willis, K. J., Szabo, A. G. & Kracjarski, D. T. Excited-state reaction and the origin of the biexponential fluorescence decay of tryptophan zwitterion. *Chem. Phys. Lett.* **182,** 614–616 (1991).
57. Kronqvist, N. *et al.* Sequential pH-driven dimerization and stabilization of the N-terminal domain enables rapid spider silk formation. *Nature Commun.* **5,** 1–11 (2014).
58. Gonnelli, M. & Strambini, G. B. Intramolecular quenching of tryptophan phosphorescence in short peptides and proteins. *Photochem. Photobiol.* **81,** 614–622 (2005).
59. Chmyrov, A., Sandén, T. & Widengren, J. Recovery of photoinduced reversible dark states utilized for molecular diffusion measurements *Anal. Chem.* **82(24),** 9998–10005 (2010).
60. Zondervan, R., Kulzer, F., Kol′chenko, M. A. & Orrit, M. Photobleaching of rhodamine 6G in poly(vinly alcohol) at the ensemble and single-molecule levels. *J. Phys. Chem. A* **108,** 1657–1665 (2004).

## Acknowledgements
This work was supported by the Swedish Research Council (VR-NT 2012-3045), the Swedish Foundation for Strategic Research (MOHICAN), and the Knut and Alice Wallenberg Foundation (KAW 2012.0218). The authors thank Jan Johansson and Nina Kronqvist, Karolinska Institutet, Stockholm, for kindly providing the NT protein.

## Author Contributions
J.W. designed research, H.H. performed experiments, J.T. developed fitting tools, H.H., J.T. and J.W. analyzed data, J.T. and J.W. wrote the manuscript. All authors discussed the results and edited the manuscript.

## Additional Information
**Supplementary information** accompanies this paper at http://www.nature.com/srep

**Competing financial interests:** The authors declare no competing financial interests.

**How to cite this article**: Hevekerl, H. *et al.* Fluorescence-based characterization of non-fluorescent transient states of tryptophan – prospects for protein conformation and interaction studies. *Sci. Rep.* **6**, 35052; doi: 10.1038/srep35052 (2016).